



Article

Ionospheric Electron Density Model by Electron Density Grid Deep Neural Network (EDG-DNN)

Zhou Chen ^{1,2}, Bokun An ^{1,2}, Wenti Liao ^{1,2}, Yungang Wang ^{3,4,*}, Rongxin Tang ^{1,2}, Jingsong Wang ⁵ and Xiaohua Deng ^{1,2}

¹ Information Engineering School, Nanchang University, Nanchang 330000, China

² Institute of Space Science and Technology, Nanchang University, Nanchang 330031, China

³ Key Laboratory of Space Weather, National Satellite Meteorological Center, China Meteorological Administration, Beijing 100081, China

⁴ Innovation Center for Fengyun Meteorological Satellite (FYSIC), Beijing 100081, China

⁵ Key Laboratory of Space Weather, National Center for Space Weather, China Meteorological Administration, Beijing 100081, China

* Correspondence: wangyg@cma.cn

Abstract: Electron density (or electron concentration) is a critical metric for characterizing the ionosphere's mobility. Shortwave technologies, remote sensing systems, and satellite communications—all rely on precise estimations of electron density in the ionosphere. Using electron density profiles from FORMOSAT-3/COSMIC (Constellation Observation System for Meteorology, Ionosphere, and Climate) from 2006 to 2013, a four-dimensional physical grid model of ionospheric electron density was created in this study. The model, known as EDG-DNN, utilizes a DNN (deep neural network), and its output is the electron density displayed as a physical grid. The preprocessed electron density data are used to construct training, validation, and test sets. The International Reference Ionosphere model (IRI) was chosen as the reference model for the validation procedure since it predicts electron density well. This work used the IRI-2016 version. IRI-2016 produced more precise results of electron density when time and location parameters were input. This study compares the electron density provided by IRI-2016 to the EDG-DNN to assess the merits of the latter. The final results reveal that EDG-DNN has low-error and strong stability, can represent the global distribution structure of electron density, has some distinctive features of ionospheric electron density distribution, and predicts electron density well during quiet periods.

Keywords: ionospheric modeling; electron density; EDG-DNN



Citation: Chen, Z.; An, B.; Liao, W.; Wang, Y.; Tang, R.; Wang, J.; Deng, X. Ionospheric Electron Density Model by Electron Density Grid Deep Neural Network (EDG-DNN).

Atmosphere **2023**, *14*, 810. <https://doi.org/10.3390/atmos14050810>

Academic Editor: Guozhu Li

Received: 30 March 2023

Revised: 20 April 2023

Accepted: 25 April 2023

Published: 29 April 2023



Copyright: © 2023 by the authors. Licensee MDPI, Basel, Switzerland. This article is an open access article distributed under the terms and conditions of the Creative Commons Attribution (CC BY) license (<https://creativecommons.org/licenses/by/4.0/>).

1. Introduction

A precise estimate of the ionospheric electron density is required for a variety of ionospheric applications, including satellite navigation, space communications, and remote sensing systems.

Due to technical observational constraints, ionosondes and high-power radars were primarily used in the early years to detect ionospheric electron density, resulting in the majority of electron density observations being concentrated at the bottom of the ionosphere in small areas and at low altitudes. A precise estimate of the ionospheric electron density is necessary for a variety of ionospheric applications, including satellite navigation, space communications, and remote sensing systems. The advancement of GPS technology has allowed detecting devices to acquire the global total electron content (TEC) property, which is the total of electron density per unit area from the bottom to the top of the ionosphere. The layered structure of the electron density is difficult to depict using TEC, and modelling based on TEC data is heavily reliant on information on three-dimensional space-time evolution (longitude, latitude, and time). As space observation technology advances, satellites carry more sophisticated observation equipment that can reverse recorded electron

density profiles into electron density data comprising height information. Using electron density data, researchers have been able to model the three-dimensional electron density of the ionosphere.

Many nations today conduct their own occultation experiments and have access to a wide range of space data products. The US Department of Defense and Taiwan together created the COSMIC (Constellation Observing System for Meteorology, Ionosphere, and Climate) program in 2006 to integrate data from various sources for ionospheric tomography. This project gave a new path to the creation of an ionosphere electron density model in four dimensions and to the realization of ionospheric tomography technology. The Constellation Observing System for Meteorology, Ionosphere, and Climate/Formosa Satellite 3 (COSMIC/FORMOSAT-3) is a joint US-Taiwan radio occultation mission consisting of six identical microsattellites. Each microsattellite carries a GPS occultation experiment (GOX) payload to operate the ionospheric radio occultation (RO) measurements [1]. The COSMIC satellites maintain an orbit of 72° inclination at an altitude of 800 km and provide 1000 to 2500 neutral atmosphere profiles and ionospheric electron density profile information per day. COSMIC has the characteristics of high vertical resolution, high precision, all-weather and long-term stability of global coverage, which can provide a large amount of valuable scientific data for ionospheric research.

Computed tomography (CT) technology was mostly used in biology and medicine in the beginning, with remarkable success. Later, researchers used satellite radio signals and CT technologies to examine the space-time distribution of ionospheric electron density. In order to reflect the vertical structure of the ionosphere without using GPS, Austen et al. originally developed ionospheric tomography (CIT) [2]. Ionospheric tomography was given a boost by Raymund et al.'s introduction of the multiplicative algebraic reconstruction technique (MART) [3]. The multiplicative algebraic reconstruction method has been used by certain researchers to perform ionospheric tomography and successfully recreate the ionospheric electron density [4–7]. Tomography was used by Pryse et al. to create the electron density image of the Svalbard archipelago polar cap region [8].

After the establishment of the GNSS constellation, the GNSS-based ionospheric tomography technology made a breakthrough in reconstructing the four-dimensional structure of the ionosphere and overcoming the limitations of the three-dimensional electron density model. Based on GPS/MET occultation data and IGS observations, Rius and others realised the real three-dimensional tomography using the Kalman filtering method [9]. Later, many scholars established several GNSS ionospheric tomography models on this basis. These models can be divided into function-based ionospheric tomography models and pixel-based ionospheric tomography models. Both function-based and pixel-based models have their advantages and disadvantages.

The potential improvements of GNSS-based ionospheric tomography at a global scale by combining the upcoming LEO constellations are investigated in Ren X et al.'s paper [10]. In terms of function basis, Amerian et al. used two-dimensional Hale wavelet and empirical orthogonal function as basis functions, respectively, to simulate the horizontal and vertical structures of the electron density and propose the solution using the truncated singular value decomposition (TSVD) method [11]. In terms of pixel basis, Chartier has proposed a tomography method that integrates GPS observation data and altimeter data [12]. Edward et al. have presented the main results of GPS/GLONASS radio sounding of ionospheric disturbances of natural and anthropogenic origin [13]. The observation of the ionosphere has never stopped, and the means are becoming more and more abundant. Today, a variety of observations of ionospheric data provide a wealth of useful data for studying the ionosphere and electron density. The four-dimensional fine modelling of ionospheric electron density based on a variety of observational data has gradually become a new development direction of ionospheric electron density research.

With its powerful computational and data-learning capabilities, deep learning can effectively process large amounts of data, and therefore has significant advantages in dealing with data-heavy electron density profiles. Many studies are now using deep

learning to study various features of the ionosphere; using deep-learning neural networks, high-accuracy ionospheric electron density modelling can be achieved.

Ma et al. proposed a residual minimisation-based training neural network method to reconstruct the three-dimensional ionospheric electron density distribution in local areas, using ionospheric sounding data to improve the vertical resolution [14]. Habarulema et al. (2011) proposed a neural network-based predictive model for ionospheric TEC modelling in South Africa and developed a global 3-D electron density reconstruction based on COSMIC 2006–2019 data and neural networks [15,16]. They found that the model based only on the COSMIC dataset was able to reproduce different ionospheric features. Ahmad Muhammad et al. used statistical and machine-learning methods to simultaneously study the relationship between earthquakes, radon gas (Rn), and total electron content (TEC) [17]. Aleksei Zhukov, et al. proposed a data-driven machine-learning approach for the total ionospheric electron content and compared it with a conventional linear regression model: the machine learning achieved $RMSE \sim 2TECU$, while the linear regression model based on significant features resulted in $\sim 4TECU$ [18]. Song et al. proposed an improved neural network based on a genetic algorithm to predict TEC in China [19]. It overcomes the problem that traditional neural networks tend to fall into in local optimization and establishes a TEC model to control the error within a certain range. Chen et al. applied deep convolutional generative adversarial networks (DCGAN) to complement TEC pictures and constructed four LSTM-based algorithms to predict the global TEC map from 2011 to 2019 [20,21]. Cesaroni et al. used the neural network method to predict the TEC of stations in different geographical locations in the world and established the global TEC model [22]. Because electron density just adds height to latitude, longitude, and time, deep learning can potentially process electron density data.

At present, deep learning is mainly used in the modelling of TEC, but it is relatively less used in the modelling of electron density. In this paper, based on deep learning, a four-dimensional electron density model is established using a physical lattice neural network to study the distribution characteristics of electron density.

2. Materials and Methods

2.1. Data Source and Preprocessing

The COSMIC dataset is available from the COSMIC Data Analysis and Archive Centre (CDAAC, <http://www.cosmic.ucar.edu>, accessed on 12 June 2022). The data used in this study are second-level data provided by CDAAC-IONPRF files, which contain information on ionospheric electron density profiles. FS-3/COSMIC can provide 2000–2500 RO measurements per day, and more than 70% of the RO measurements can be successfully converted into electron density profiles, which are one of the most important products for space weather and ionospheric science. Tsai et al. describe the derivation of ionospheric electron density from RO measurements in detail [23]. The Abel inversion is often used to convert TEC data into electron density data. A generalised quadrature method has been proposed by V. S. Sizikov et al. for the numerical solution of Abel-type singular integral equations, which simplifies the problem of solving singular integral equations [24]. It should be noted that a number of factors can affect the quality of the electron density data. The error of the electron density is derived from RO measurements, including the measurement errors and the error during the Abel inversion. Yue et al. have found that the electron density derived by the Abel inversion method has a large error at low latitudes and a higher accuracy at midlatitudes and high latitudes [25]. A study of the source of error by Wu et al. shows that measurement errors can hardly affect the accuracy of the electron density [26].

Figure 1 shows the distribution of electron density data on 12 January 2010. Figure 1a shows that the electron density trajectories are almost uniformly distributed in the ionosphere, with less distribution in the polar regions as shown in Figure 2; Figure 1b shows the vertical distribution of electron density trajectories from 100 km to 800 km. The dataset used for this study spans from the 113th day of 2006 to the last day of 2013. The dataset's

negative values were eliminated in order to preserve the expected positive electron density values, which were then recorded as an NPY file for each year’s electron density data.

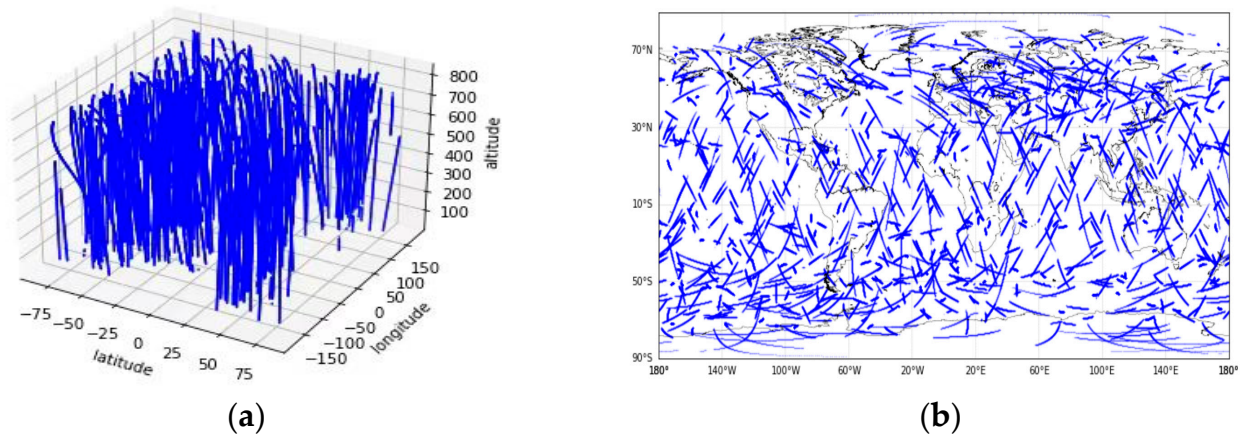


Figure 1. Example of the global distribution of the COSMIC trajectory visualisation during 12 January 2010: (a) 3-D distribution of the electronic density trace; (b) horizontal distribution of the electronic density trace.

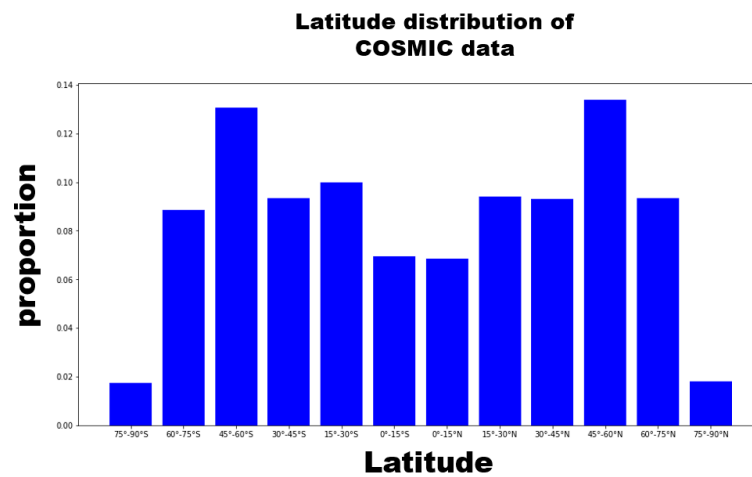


Figure 2. Distribution of electron density over longitude, spanning 15° latitude.

2.2. IRI-2016 Model

The International Reference Ionosphere (IRI) is an international project that is jointly established by the Committee on Space Research (COSPAR) and the International Union of Radio Science (URSI) [27].

The IRI model is an empirical ionospheric model that is based on data from ionospheric vertical observing stations and satellite observations. Its goal is to offer systematic and all-encompassing ionospheric parameters. The IRI model may anticipate electron density data in a steady manner and serve as a reference for the four-dimensional ionospheric electron density model.

The IRI-2016 version is used in this study, which operates in a Linux Python environment. To utilize it, it was installed, and the iri2016 module package was invoked in a Jupyter Notebook. To acquire electron density data, the corresponding longitude, latitude, altitude, and time were entered. The performance of EDG-DNN was assessed by comparing it with the IRI-2016 prediction results.

2.3. COSMIC_DNN Model Introduction

The purpose of this paper is to build a four-dimensional gridded electron density model with longitude, latitude, altitude, and time using a deep-learning neural network and the COSMIC electron density data profiles.

The electron density data in the ionospheric electron density profiles are large and discrete across the entire ionospheric space, making it difficult to obtain a global ionospheric model with high resolution and covering time and space using traditional mathematical methods. Deep learning, on the other hand, has powerful data-processing capabilities that allow a DNN to understand the distribution features of the data as well as the relationship between the data, and thus obtain a gridded global electron density distribution from the irregular input.

Figure 2 shows the basic algorithm flow of DNN. The internal structure of the DNN algorithm is very similar to the traditional neural network algorithm, which mainly consists of the input layer, hidden layer, and output layer. Information is transmitted between layers in a fully connected manner. DNN adopts forward propagation and directional propagation algorithms, so it has significant advantages in data fitting.

The input matrix of the input layer (X) and the input matrix of the hidden layer (A) can be expressed as:

$$X = \begin{bmatrix} x_1 \\ x_2 \\ \vdots \\ x_m \end{bmatrix}, A = \begin{bmatrix} a_1 \\ a_2 \\ \vdots \\ a_n \end{bmatrix}$$

The weight of each input (x_i) of the input layer corresponding to each hidden layer (a_j) is w_{ij} , so the weight matrix (W) is expressed as:

$$W = \begin{bmatrix} w_{11} & \cdots & w_{1n} \\ \vdots & \ddots & \vdots \\ w_{m1} & \cdots & w_{mn} \end{bmatrix}$$

Through the action of neurons, the above formula is expressed as:

$$h_i = [w_{1i} \quad w_{2i} \quad \cdots \quad w_{mi}] * \begin{bmatrix} x_1 \\ x_2 \\ \vdots \\ x_m \end{bmatrix}$$

In addition to the output layer, each neuron in the hidden layer must be activated by the activation function and output to the next neuron, so the formula can be expressed as:

$$H = W^T X + [b]$$

$$p_i = g(h_i)$$

where p_i is the output of neurons and b is the bias unit. Using the same method for the next hidden layer or output layer, the value distributed between 0 and 1 in the output layer can be obtained.

The more hidden layers, the better the generalisation ability of the network and the better the fitting effect, but the complexity of the network will increase accordingly and the training time will increase significantly. For shallow networks, increasing the network width, i.e., the number of hidden layer nodes, can improve the generalisation ability and the fitting effect, but it has little effect on more complex networks. Bengio et al. found that decreasing the network depth leads to an exponential increase in the number of computational elements used to fit the function [28]. This means that increasing

the network depth is more effective than increasing the width. The use of five hidden layers allows the model to run with the intended effect while maintaining the model’s computational efficiency. After altering the hidden layer nodes, it is discovered that the model performs best when the number of nodes is 256, 128, 64, 16, and 4, respectively.

The input dimension is (8,1), and each data are composed of longitude, latitude, altitude, year, day of the year (doy), hour, minute, and corresponding electron density, where the time is Universal Standard Time (UT). Since Solar Zenith Angle (SZA) refers to the angle between the direction of incoming solar radiation and the zenith, which determines the amount of solar thermal energy that can be obtained by ionospheric components and can affect the degree of ionisation of neutral components, it is closely related to the distribution of electron density. Therefore, SZA is also added to the data to strengthen the constraints.

The activation function used in this study was *RELU*. When the input is x , *RELU* can be expressed as:

$$\sigma(x) = RELU(x) = \begin{cases} 0, & x \leq 0 \\ x, & x > 0 \end{cases}$$

RELU has a fast computation speed and its convergence speed is much faster than sigmoid. It can solve the gradient disappearance problem.

The optimisation algorithm used in this study was Adam (adaptive moment estimation). Adam can efficiently solve the problem of local deep learning, and the effect is better than other random algorithms [29].

The electron density dataset used in this study spans the years 2006 to 2013, and the electron density profiles for each year are combined into a single file. The data from each year are separated into training, validation, and test sets in the ratio of 8:1:1. The training and validation sets are combined and trained for a total of 500 epochs, and the batch size is set to 5120, using the loss function MAE (mean absolute error loss) utilized in the training. ReduceLROnPlateau from Keras is used in the study to automatically adjust the learning rate, with an initial learning rate of 0.1 and MAE as monitor; when MAE has 20 epochs without change, the learning rate is adjusted to 1/2 of the original. Figure 3 depicts the composition structure and basic algorithm of the neural network. Figure 4 shows the loss variation curves of the training and validation sets. Figure 5 depicts the entire model process from input to output.

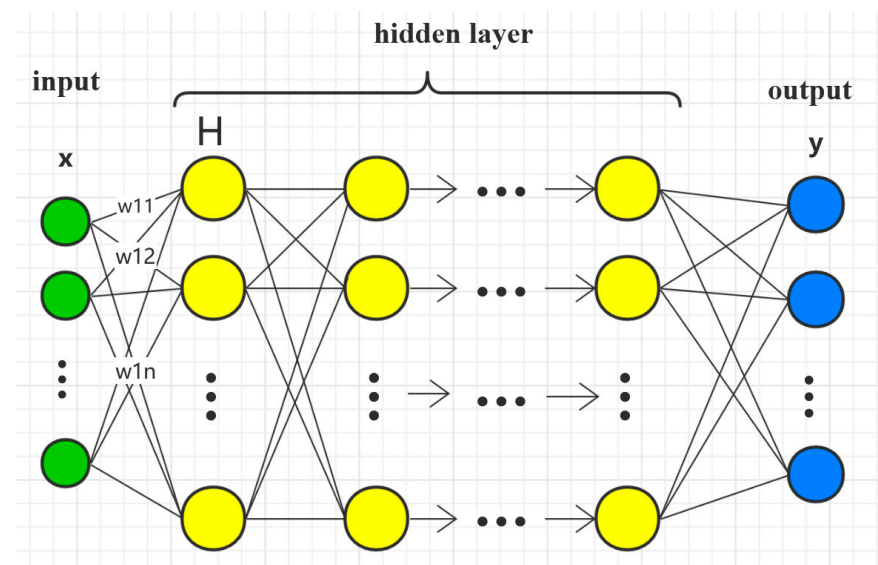


Figure 3. Composition and basic algorithm of DNN neural network.

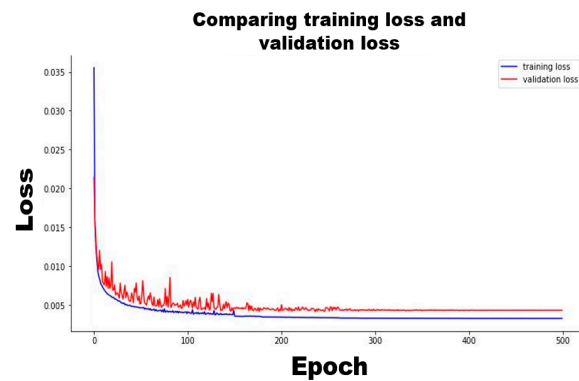


Figure 4. Loss changes in the training and validation sets during training. The blue curve is the loss change in the training set and the red curve is the loss change in the validation set.

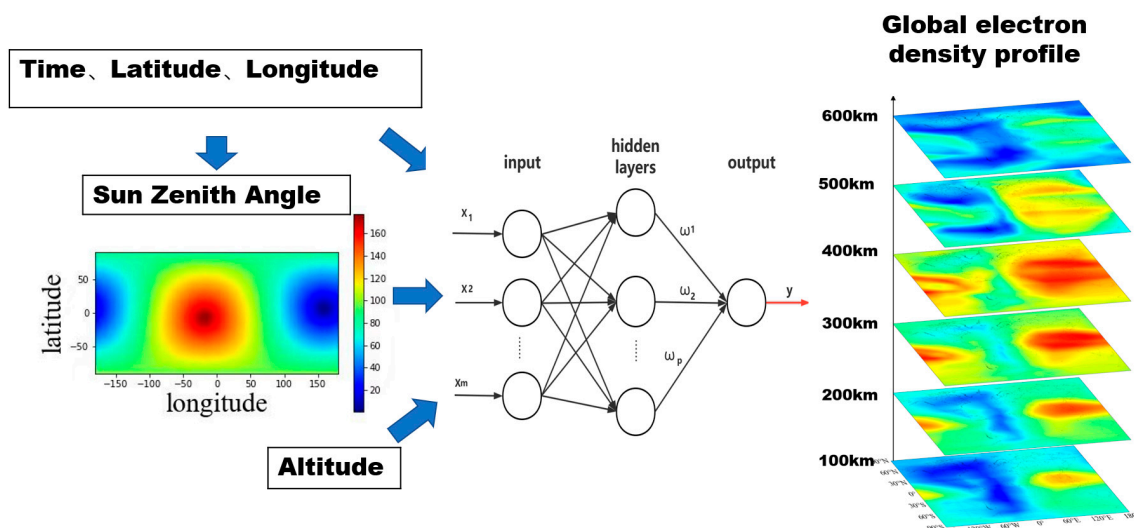


Figure 5. The flowchart of the EDG-DNN model shows the ionospheric tomography on 20 March 2012: the inputs are on the left, the main structure of the DNN is in the middle, and the output of the physical gridding is on the right.

The data in the test set will be used to test the prediction effect of EDG-DNN, analyze EDG-DNN by comparing the effect with IRI-2016, and demonstrate the effect of the model response to the magnetic storm period by comparing the change in ionospheric electron density before and after the magnetic storm.

3. Results

This study employs *RMSE* (root mean square error) and *MAD* (mean absolute deviation) to examine the bias of the EDG-DNN model since the validation of predictive models necessitates assessment metrics to precisely measure the reliability and validity of the models. These are their mathematical expressions:

$$RMSE = \sqrt{\frac{1}{n} \times \sum_{i=1}^n (F_i - O_i)^2} \tag{1}$$

$$MAD = \frac{1}{n} \sum_{i=1}^n |F_i - O_i| \tag{2}$$

where F_i represents the predicted electron density, which is produced by models, O_i represents the COSMIC electron density.

3.1. Comparison with COSMIC Electron Density Data and IRI-2016

During the testing, the study compared the performance effect of EDG-DNN with IRI-2016.

Figure 6 verifies the prediction effect of the electron density of the EDG-DNN model on 20 March 2012 and 20 September 2012. The first row is the comparison of the electron density distribution of the COSMIC trajectories and the prediction effects of the EDG-DNN model and the IRI-2016 model, expressed in red, blue, and green, respectively. The second row is the distribution of the difference between the EDG-DNN and IRI models and the COSMIC electron density trajectories, expressed in blue and green, respectively. The IRI-2016 tends to underestimate the electron density in the ionospheric region below 300 km and slightly overestimate the electron density in the ionospheric region above 300 km at the vernal equinox, while the error between the EDG-DNN and COSMIC electron densities remains small and stable. The EDG-DNN and IRI models have root mean square errors of 0.587 and 0.993, respectively. The prediction effects of the EDG-DNN model and the IRI-2016 model are similar during the autumnal equinox, and the errors of the EDG-DNN model and the IRI-2016 model are kept within a limited range with those of the COSMIC electron density trajectories. The IRI-2016 model, on the other hand, has some individual electron density prediction mistakes. The EDG-DNN model and the IRI model have root mean square errors of 0.453 and 0.471, respectively. As a result, in most circumstances, EDG-DNN’s prediction performance is comparable to that of COSMIC electron density trajectories and better than that of the IRI-2016 model.

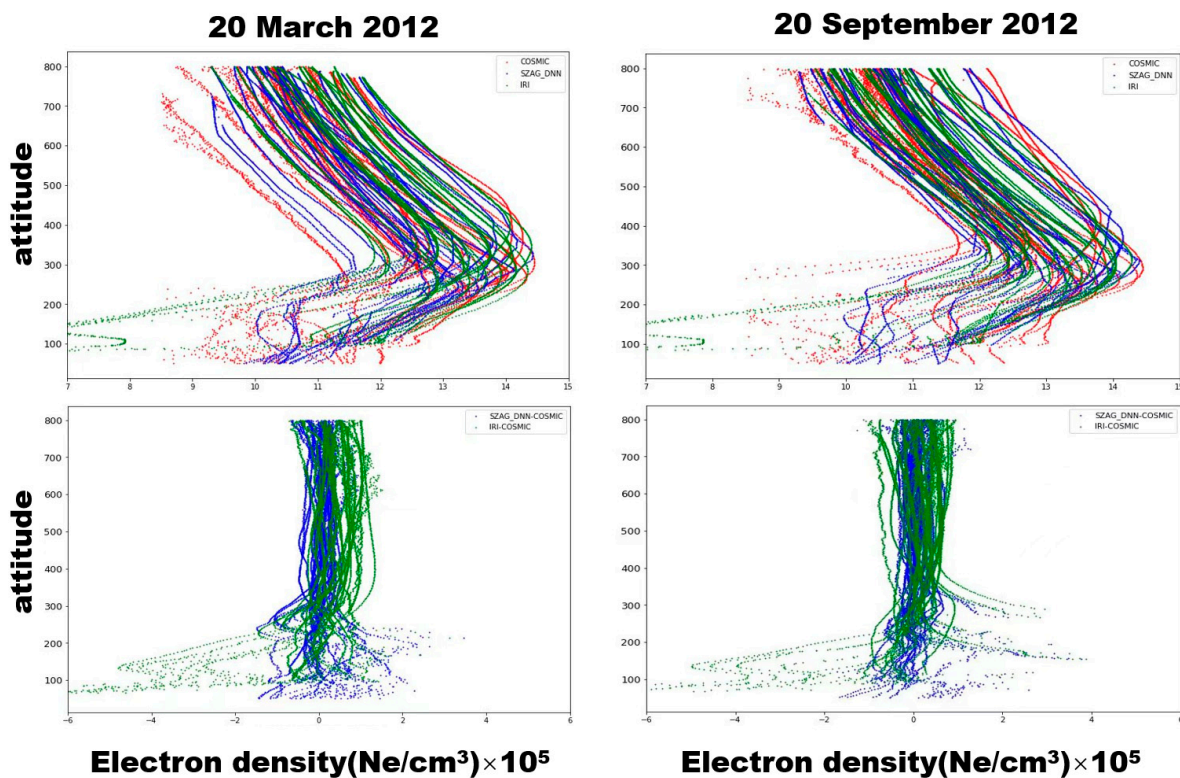


Figure 6. Row 1: SZA-DNN and IRI-2016 predict electron density and COSMIC trajectory electron density distribution. Row 2: Distribution of electron density difference of EDG-DNN, IRI-2016, and COSMIC trajectories.

The average *RMSE* and *MAD* for EDG-DNN and IRI-2016 at various latitudes around the world are shown in Table 1. EDG-DNN performs better at midlatitudes than at high latitudes because of fewer electron density profiles distributed at high latitudes, allowing the model to obtain relatively less information through learning, and probably because of

the more complex ionospheric motion at high latitudes. The average *RMSE* and *MAD* of EDG-DNN at different latitudes are always lower than those of IRI.

Table 1. The averaged performance of models on the test set.

Latitude	EDG-DNN Model		IRI-2016 Model	
	<i>MAD</i>	<i>RMSE</i>	<i>MAD</i>	<i>RMSE</i>
70° S–90° S	0.877	0.992	0.979	1.158
50° S–70° S	0.339	0.424	0.495	0.633
30° S–50° S	0.434	0.503	0.368	0.414
10° S–30° S	0.462	0.579	0.559	0.629
10° S–10° N	0.415	0.575	0.746	0.893
10° N–30° N	0.424	0.523	0.628	0.751
30° N–50° N	0.311	0.407	0.511	0.609
50° N–70° N	0.285	0.353	0.399	0.457
70° N–90° N	0.726	0.819	1.002	1.201

3.2. Changes of Electron Density during Magnetic Storms

Figure 7 shows the electron density change during a magnetic storm in September 2011 as reproduced by the EDG-DNN model. It can be seen from Figure 7b that the electron density changed dramatically during the magnetic storm period, and the electron density at noon in local time increased greatly compared with that in the quiet period. The vertical electron density data are superimposed in Figure 7a, and it can be seen that the peak value of the electron density during the magnetic storm is higher than the peak value in the quiet period, and the trough value is lower than the trough value of the electron density in the quiet period. This shows that EDG-DNN can reproduce the characteristics of the electron density changing with time during the magnetic storm to a certain extent.

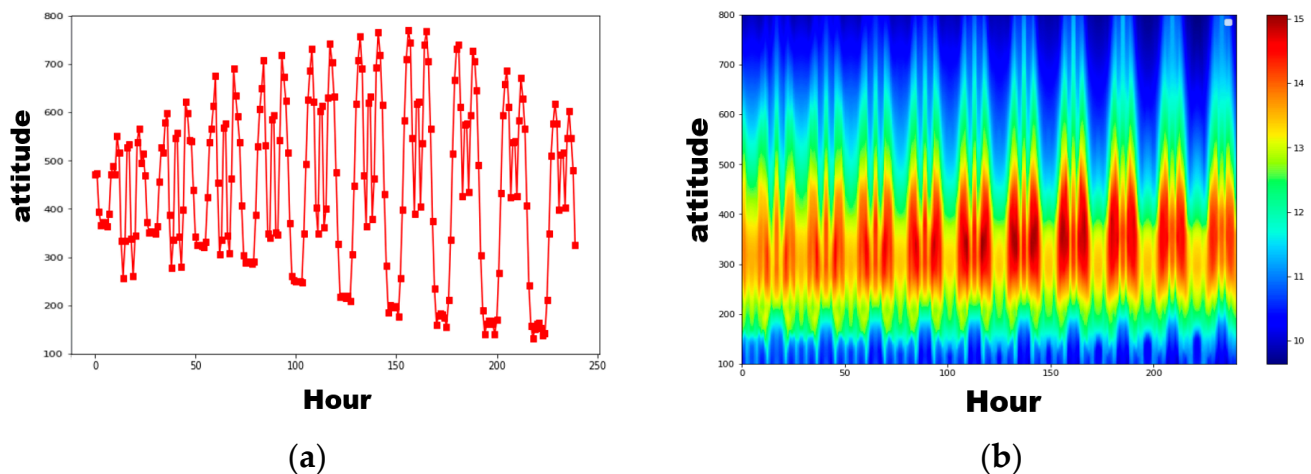


Figure 7. Change of electron density profile from 15 to 24 September 2011: (a) shows the change of electron density after the superposition of vertical electron density; (b) shows the vertical heat map of electron density at the ionosphere from 100 km to 800 km (28° N, 115° E).

3.3. Global Distribution Characteristic of Ionospheric Electron Density

Figure 8 compares the ionospheric electron density tomography of the EDG-DNN model and the IRI model on 20 March 2012 and 20 September 2012, respectively, at an altitude of 300 km. The equatorial bimodal structure may be detected in the EDG-DNN tomography at all times. Areas with high electron density shift as the sun's angle of incidence changes throughout the day. This modification is well represented by EDG-DNN, which is congruent with the IRI-2016 model. The EDG-DNN model and the IRI model are very comparable in most places; however, the difference graph demonstrates that the

prediction effect of EDG-DNN in these regions deviates significantly from the IRI model. These variations are scattered throughout different regions, which does not indicate that the prediction findings are biased. Because the IRI-2016 model is empirical, it tends to represent the statistical features of the electron density; hence, it loses the local properties of the electron density. The COSMIC data utilized by EDG-DNN can represent more detailed features than the IRI-2016 model. The results reveal that the EDG-DNN model predicts the electron density distribution well and can capture the general structure of the ionospheric electron density distribution.

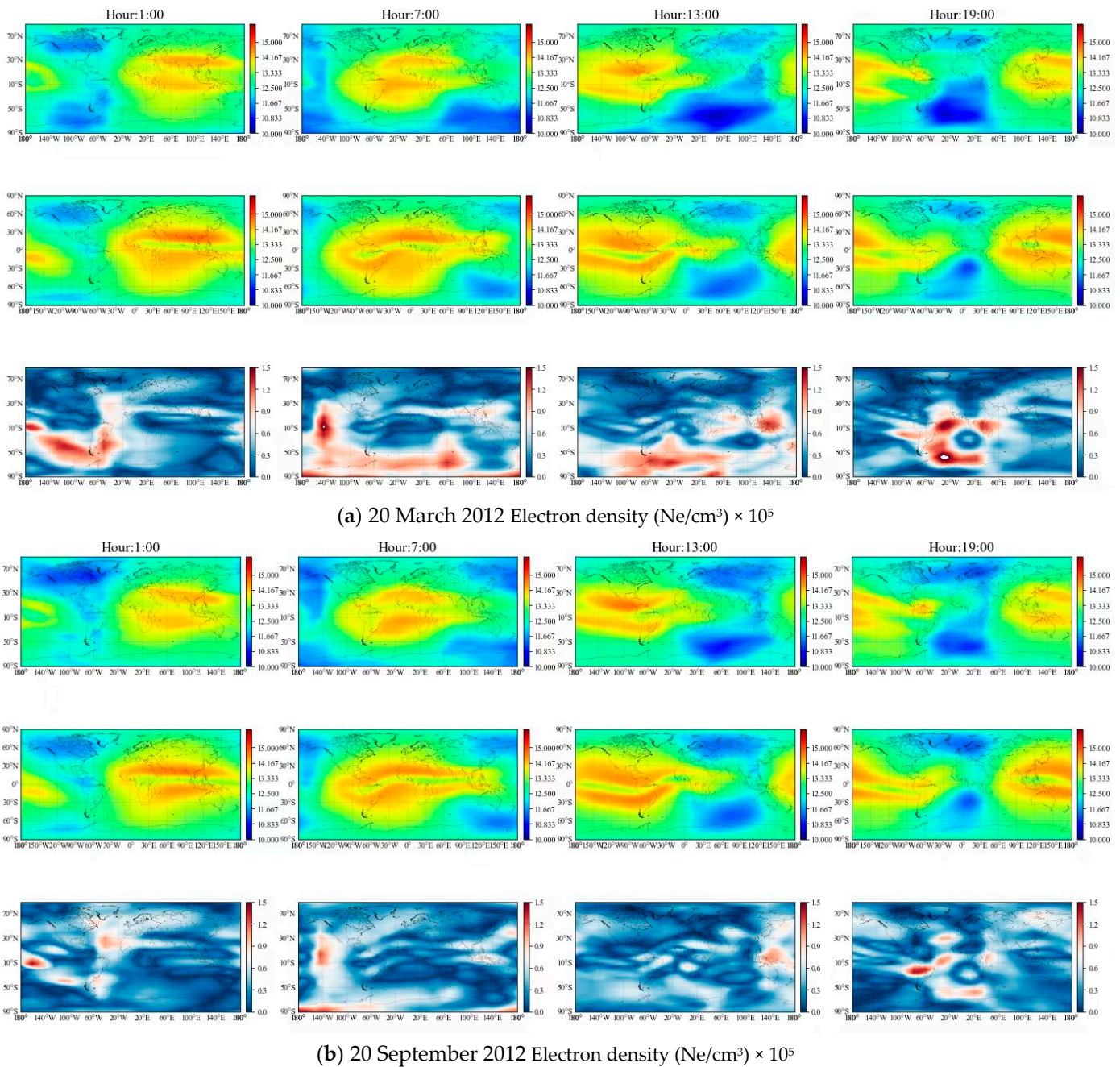


Figure 8. Comparison of global electron density tomography by EDG-DNN (first row) and IRI-2016 (second row), and the third line is the difference between the two: (a) shows the electron density tomogram on 20 March 2012; (b) shows the electron density tomogram on 20 September 2012.

4. Discussion

Using cosmic occultation data and a deep neural network, a four-dimensional electron density grid model (EDG-DNN) based on longitude, latitude, altitude, and time was created in this study. Furthermore, the prediction effect has been extensively compared with IRI-2016 based on the test set. The results show that the EDG-DNN performs with good stability and error.

5. Conclusions

Based on the above results, our conclusions are as follows:

1. The EDG-DNN model can present a gridded ionospheric electron density distribution with more accurate predictions. It can also be used as a reliable electron density reference model for further studies of the ionosphere.
2. The EDG-DNN model learns the distribution features of a vast quantity of electron density data in order to better depict the structure of the ionosphere, such as the equatorial bimodal structure, in the forecast. It can also reflect the electron density variation and distribution during magnetic storms to some extent, which is important for further research into the electron density variation and dispersion during magnetic storms.

This study shows that DNN can be used to build a four-dimensional electron density model of the ionosphere. This demonstrates that deep learning can be applied to a wider range of earth sciences, particularly to the problem of predicting features such as ionospheric electron density. In the future, the study plans to use more accurate deep-learning models and electron density data to obtain better electron density models, be more accurate in predicting electron density, construct detailed electron density features during magnetic storms, and analyse and predict electron density during storms.

Author Contributions: Conceptualization, Z.C.; Methodology, Z.C.; Software, Z.C. and B.A.; Validation, Z.C. and B.A.; Formal analysis, B.A. and W.L.; Investigation, B.A. and W.L.; Resources, W.L. and R.T.; Data curation, R.T.; Writing—review & editing, Y.W.; Visualization, X.D.; Project administration, J.W.; Funding acquisition, J.W. All authors have read and agreed to the published version of the manuscript.

Funding: This work is funded by the National Natural Science Foundation of China (grants no. 41974183, 41974195, 41774195, 41604136 and 41674144), and the Interdisciplinary Innovation Fund of Natural Science from Nanchang University (grant no. 9166-27060003-YB14).

Institutional Review Board Statement: Not applicable.

Informed Consent Statement: Not applicable.

Data Availability Statement: Some of the processed data and code files used in this study have been uploaded to the website <https://osf.io/2dzk7/>, accessed on 1 February 2023.

Acknowledgments: The COSMIC dataset can be available from the COSMIC Data Analysis and Archive Center (CDAAC, <http://www.cosmic.ucar.edu/>, accessed on 12 June 2022). We are thankful to the website for providing data for our research.

Conflicts of Interest: The authors declare no conflict of interest.

References

1. Cherniak, I.; Zakharenkova, I. Validation of FORMOSAT-3/COSMIC radio occultation electron density profiles by incoherent scatter radar data. *Adv. Space Res.* **2014**, *53*, 1304–1312. [\[CrossRef\]](#)
2. Austen, J.R.; Franke, S.J.; Liu, C.H.; Yeh, K.C. Application of computerized tomography techniques to ionospheric research. In Proceedings of the International Beacon Satellite Symposium on Radio Beacon Contribution to the Study of Ionization and Dynamics of the Ionosphere and to Corrections to Geodesy and Technical Workshop, Oulu, Finland, 9–14 June 1986; Tauriainen, A., Ed.; Part 1 (A87–50101 22–46); University of Oulu: Oulu, Finland, 1986; pp. 25–35.
3. Raymund, T.D.; Austen, J.R.; Franke, S.J.; Liu, C.H.; Klobuchar, J.A.; Stalker, J. Application of computerized tomography to the investigation of ionospheric structures. *Radio Sci.* **1990**, *25*, 771–789. [\[CrossRef\]](#)

4. Heaton, J.A.T.; Pryse, S.E.; Kersley, L. Improved background representation, ionosonde input and independent verification in experimental ionospheric tomography. *Ann. Geophys.* **1995**, *13*, 1297–1302. [[CrossRef](#)]
5. Kersley, L.; Heaton, J.A.T.; Pryse, S.E.; Raymund, T.D. Experimental ionospheric tomography with ionosonde input and EISCAT verification. *Ann. Geophys.* **1993**, *11*, 1064–1074. [[CrossRef](#)]
6. Mitchell, C.N.; Jones, D.G.; Kersley, L.; Pryse, S.E.; Walker, I.K. Imaging of field-aligned structures in the auroral ionosphere. *Ann. Geophys.-Eur. Geophys. Soc.* **1995**, *13*, 1311–1319.
7. Vasicek, C.; Kronschnabl, G. Ionospheric tomography: An algorithm enhancement. *J. Atmos. Terr. Phys.* **1995**, *57*, 875–888. [[CrossRef](#)]
8. Pryse, S.; Kersley, L.; Williams, M.; Walker, I.; Willson, C. Tomographic imaging of the polar-cap ionosphere over svalbard. *J. Atmos. Solar-Terr. Phys.* **1997**, *59*, 1953–1959. [[CrossRef](#)]
9. Rius, A.; Ruffini, G.; Cucurull, L. Improving the vertical resolution of ionospheric tomography with GPS Occultations. *Geophys. Res. Lett.* **1997**, *24*, 2291–2294. [[CrossRef](#)]
10. Ren, X.; Mei, D.; Zhang, X.; Freeshah, M.; Xiong, S. Electron Density Reconstruction by Ionospheric Tomography From the Combination of GNSS and Upcoming LEO Constellations. *J. Geophys. Res. Space Phys.* **2021**, *126*, e2020JA029074. [[CrossRef](#)]
11. Erturk, O.; Arikan, O.; Arikan, F. Tomographic Reconstruction of the Ionospheric Electron Density in terms of Wavelets. *Iran. Aerosp. Soc.* **2010**, *43*, 1702–1710.
12. Chartier, A.T.; Smith, N.D.; Mitchell, C.N.; Jackson, D.R.; Patilongo, P.J.C. The use of ionosondes in GPS ionospheric tomography at low latitudes. *J. Geophys. Res. Atmos.* **2012**, *117*, A10326. [[CrossRef](#)]
13. Afraimovich, E.L.; Astafyeva, E.I.; Demyanov, V.; Edemskiy, I.; Gavriluk, N.S.; Ishin, A.; Kosogorov, E.A.; Leonovich, L.A.; Lesyuta, O.S.; Palamartchouk, K.; et al. A review of GPS/GLONASS studies of the ionospheric response to natural and anthropogenic processes and phenomena. *J. Space Weather Space Clim.* **2013**, *3*, A27. [[CrossRef](#)]
14. Ma, X.F.; Maruyama, T.; Ma, G.; Takeda, T. Three-dimensional ionospheric tomography using observation data of GPS ground receivers and ionosonde by neural network. *J. Geophys. Res. Atmos.* **2005**, *110*, A05308. [[CrossRef](#)]
15. Habarulema, J.B.; Mckinnell, L.; Opperman, B. Regional Ionospheric TEC Modelling; Working towards Mapping Africa's Ionosphere. In *General Assembly & Scientific Symposium*; IEEE: Washington, DC, USA, 2011.
16. Habarulema, J.B.; Okoh, D.; Burešová, D.; Rabiú, B.; Tshisaphungo, M.; Kosch, M.; Häggström, I.; Erickson, P.J.; Milla, M.A. A global 3-D electron density reconstruction model based on radio occultation data and neural networks. *J. Atmos. Solar-Terr. Phys.* **2021**, *221*, 105702. [[CrossRef](#)]
17. Muhammad, A.; Kùlahcı, F.; Birel, S. Investigating radon and TEC anomalies relative to earthquakes via AI models. *J. Atmos. Solar-Terr. Phys.* **2023**, *245*, 106037. [[CrossRef](#)]
18. Zhukov, A.; Sidorov, D.; Mylnikova, A.; Yasyukevich, Y. Machine Learning Methodology for Ionosphere Total Electron Content Nowcasting. *Int. J. Artif. Intell.* **2018**, *16*, 144–157. [[CrossRef](#)]
19. Song, R.; Zhang, X.; Zhou, C.; Liu, J.; He, J. Predicting TEC in China based on the neural networks optimized by genetic algorithm. *Adv. Space Res.* **2018**, *62*, 745–759. [[CrossRef](#)]
20. Chen, Z.; Jin, M.; Deng, Y.; Wang, J.; Huang, H.; Deng, X.; Huang, C. Improvement of a Deep Learning Algorithm for Total Electron Content Maps: Image Completion. *J. Geophys. Res. Space Phys.* **2019**, *124*, 790–800. [[CrossRef](#)]
21. Chen, Z.; Liao, W.; Li, H.; Wang, J.; Deng, X.; Hong, S. Prediction of Global Ionospheric TEC Based on Deep Learning. *Space Weather* **2022**, *20*, e2021SW002854. [[CrossRef](#)]
22. Cesaroni, C.; Spogli, L.; Aragon-Angel, A.; Fiocca, M.; Dear, V.; De Franceschi, G.; Romano, V. Neural network based model for global Total Electron Content forecasting. *J. Space Weather Space Clim.* **2020**, *10*, 11. [[CrossRef](#)]
23. Tsai, L.C.; Tsai, W.H.; Schreiner, W.S.; Berkeley, F.T.; Liu, J.Y. Comparisons of GPS/MET retrieved ionospheric electron density and ground based ionosonde data. *Earth Planets Space* **2001**, *53*, 193–205. [[CrossRef](#)]
24. Sizikov, V.; Sidorov, D. Generalized quadrature for solving singular integral equations of Abel type in application to infrared tomography. *Appl. Numer. Math.* **2016**, *106*, 69–78. [[CrossRef](#)]
25. Yue, X.; Schreiner, W.S.; Lei, J.; Sokolovskiy, S.V.; Rocken, C.; Hunt, D.C.; Kuo, Y.H. Error analysis of Abel retrieved electron density profiles from radio occultation measurements. In *Annales Geophysicae: Atmospheres, Hydrospheres and Space Sciences*; Copernicus Publications: Göttingen, Germany, 2010.
26. Wu, X.; Hu, X.; Gong, X.; Zhang, X.; Wang, X. Analysis of inversion errors of ionospheric radio occultation. *GPS Solut.* **2009**, *13*, 231–239. [[CrossRef](#)]
27. Bilitza, D.; Altadill, D.; Zhang, Y.; Mertens, C.J.; Truhlik, V.; Richards, P.; McKinnell, L.-A.; Reinisch, B.W. The International Reference Ionosphere 2012—A model of international collaboration. *J. Space Weather Space Clim.* **2014**, *4*, A07. [[CrossRef](#)]
28. Bengio, Y.; Lecun, Y. Scaling learning algorithms towards AI. In *Large-Scale Kernel Machines*; George Mason University: Fairfax, VA, USA, 2007; pp. 321–359.
29. Kingma, D.; Ba, J. Adam: A Method for Stochastic Optimization. *arXiv* **2014**, arXiv:1412.6980.

Disclaimer/Publisher's Note: The statements, opinions and data contained in all publications are solely those of the individual author(s) and contributor(s) and not of MDPI and/or the editor(s). MDPI and/or the editor(s) disclaim responsibility for any injury to people or property resulting from any ideas, methods, instructions or products referred to in the content.